2017 IEEE International Conference on Systems, Man, and Cybernetics (SMC)
Banff Center, Banff, Canada, October 5-8, 2017

Nonlinear Workspace Mapping for Telerobotic Assistance of Upper Limb in Patients with Severe Movement Disorders

Carlos Rossa, Mohammad Najafi, and Mahdi Tavakoli
Department of Electrical and Computer Engineering
University of Alberta, Edmonton, Canada
carlos.rossa@uoit.ca; {najafi; mahdi.tavakoli}@ualberta.ca

Kim Adams
Faculty of Rehabilitation Medicine, University of Alberta
Glenrose Rehabilitation Hospital, Edmonton, Canada
kdadams@ualberta.ca

***Abstract*—Telerobotic manipulation allows patients living with upper limb impairments to interact with a variety of environments and accomplish through teleoperation daily activities such as playing, feeding, self-care, and leisure, that would otherwise be difficult to perform. In this paper, we propose a nonlinear mapping between the patient's range of motion and the workspace of an environment being manipulated. The objective is to identify the patient's workspace and span it to that of the environment or an object, thus optimizing the scaling factor while soliciting the entire patient's range of motion. The boundaries of each workspace are obtained from scattered measurements of the master and slave robots end-effector position. The nonlinear mapping is then achieved through thin plate spline interpolation that describes deformation between two surfaces by scattered point-to-point preponderances. Experimental results reported in three different scenarios confirm the suitability of the nonlinear transformation to map diverse workspace volumes.**

I. Introduction

It is estimated that about 460,000 Canadians are living with the effects of stroke [1], and more than 500,000 Americans under the age of 18 have at least one cerebral palsy symptom that negatively affects daily life tasks [2]. Symptoms associated with these disabilities often include loss of motor control, reduced mobility, restricted range of motion, joint stiffness, and difficulties in performing movements [3]. Due to the aging population in Canada and growing population in the USA, the need for therapeutic services is expected to significantly increase in the near future [1], [4]. Recent development in the field of robotics has opened new avenues for patients affected by such severe movement disorders. Assistive robotic technologies are used to compensate for disabilities due to a given pathological condition while minimizing the social disadvantages related to it.

One of the most prominent paradigms in robotic assistance is single or multiuser teleoperation of robotic manipulators. The former allows a patient living with impairments of upper limb movements to accomplish through teleoperation activities of daily living, such as feeding, and leisure, that would otherwise be difficult or impossible to perform [5]. Typically, the individual controls a dexterous manipulator (slave robot) using a chair-mounted joystick or a haptic device (master robot) [6]. Such teleoperation schemes are often implemented through position control in which the displacement of the slave robot end-effector is directly correlated to displacement of the master robot. Since the workspace of each robot is different from the other, the motion may be scaled according to a mapping from the device position [7], [8].

Multi-user bilateral teleoperation, on the other hand, allows patients to perform tasks cooperatively with other individuals. These systems give access to activities that are known to play an important role in the development of young patient's cognitive and perceptual skills [9], [10]. Patients with more motivation in such tasks are believed to have higher motor recovery and improvement of symptoms than those described as less enthusiastic [11], [12]. In this regard, intuitive coordinated interaction between patient and the environment of the slave robot is a key factor that can influence patient engagement and the associated benefits of these activities [13].

The question then arises on how to scale the workspaces of a patient with limited range of motion to that of an individual without disability or a given environment. To illustrate this issue consider the teleoperated robotic scheme depicted in Fig. 1. The motion executed with the master robot is scaled up or down to match the workspace of the slave robot, such that the whole range of the patient's workspace is explored. For instance, assume that a patient with a spastic arm is controlling the master robot. One defining feature of spasticity is known as hypertonia; a condition in which muscle tone drastically increases making joints stiff and difficult to move, typically assuming a flexed position [14]. If the patient is unable to move the flexed elbow, the reachable workspace is likely to form a C-like shape (W_p in Fig. 1). Thus, a simple linear scale between the two workspaces is not appropriate.

Scaling down the patient workspace to match a constrained workspace such as that of a small object refines the patient motion and allows for precise motion of the slave end-effector. This can be considered for patients with movement spasms attempting to perform a precise motion in a small workspace such as stirring a mug. Scaling up the patient workspace amplifies the patient's motion and allows him to perform tasks in a workspace that he would otherwise not be able to reach. However, upscaling works well for coarse motion but for tasks

978-1-5386-1644-4/17/$31.00 ©2017 IEEE

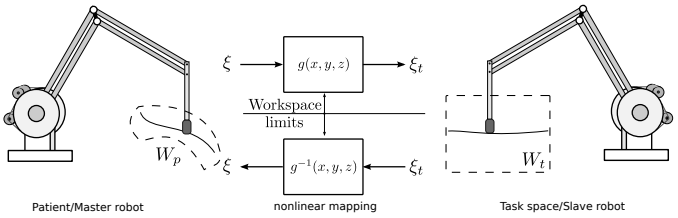

Fig. 1. Unilateral teleoperation. The patient workspace W_p (master robot on the left) is to be mapped to that of the slave robot (W_t) through a nonlinear position interpolation function g. The transformed three-dimensional position of the master end-effector ξ is the desired position of the slave robot ξ_t. The interpolation only depends on the outline of the workspaces.

in which accurate positioning of the slave is needed, large scaling of the patient movement subject to involuntary movement makes a target acquisition task physically impossible [7].

In this paper, we develop a nonlinear workspace mapping to assist with telemanipulation of objects by a patient's. The objective is to identify the entire patient's workspace and span it to that of the object, thus limiting the scaling factor and soliciting the patient's motion. The nonlinear scaling is achieved through thin plate spline interpolation where reference points in both workspaces are defined and the workspace is deformed until the reference points are matched. The remainder of the workspace is interpolated around those points. A method is also devised to outline the limits of the workspaces by manually moving the end-effector of both robots in their desired ranges of motion. We present three different experimental scenarios. The first considers object-to-object mapping; the second and third map the workspace obtained when the patient is only able to move the wrist or the shoulder, respectively, to that of an object. Experimental results confirm the suitability of the proposed method to map highly curved workspaces and the ability of the user to outline contours and follow lines of objects despite the highly nonlinear mapping.

II. Nonlinear Workspace Mapping

Assume that the patient controls the master robot in the unilateral tele-operated scheme depicted in Fig 1. The patient's reachable workspace is denoted W_p and W_t refers to the workspace in the slave robot. We seek a transformation $g(x,y,z)$ in the three-dimensional (3D) space to match the contours of both workspaces and interpolate the robot's position within the transformed workspace.

Depending on the shape of the two workspaces, this mapping is not necessary a simple linear shape or volume scaling. Nevertheless, the goal is to map the volume/shape of W_p into that of W_t, or vice-versa, with a non-rigid transformation that minimizes the overall distortion of the workspace to be mapped. For 3D volumes, thin plate spline (TPS) interpolation has this property. TPS is an algebraic approach to the description of deformation between two surfaces specified by scattered point preponderances (landmark points) [15].

Consider the state variable $\xi = [x,y,z]^T$ defined in the Cartesian space that solely represents the 3D position of a generic point. To find the transformation $g(\xi)$ between W_p and W_t, we assume to have a set of n landmarks $\xi_r = [x_t\ y_t\ z_t]^T$ in the reference workspace (the coordinates of 3D points to be deformed to match the target workspace), and the corresponding homologous set of n landmarks ξ_t in the target workspace. This process involves deforming the reference workspace such that the reference landmarks (patient's side) match the location of target landmarks (on the slave robot side), i.e., $g(\xi_r) = \xi_t$, while minimizing a bending energy function associated with the transformation. The function $g(x,y,z) \in \mathbb{R}^3$ must be twice differentiable and minimize the distortion of the reference shape that is quantifiable by

$$\int\int\int_{\mathbb{R}^3} \left(\frac{\partial^2 g}{\partial x^2} + \frac{\partial^2 g}{\partial y^2} + \frac{\partial^2 g}{\partial z^2} \right)^2 dxdydz. \tag{1}$$

The transformation can be written as a sum of functionals which only depend on one component of g, that is:

$$g(x,y,z) = b_0 + b_1 x + b_2 y + b_3 z + \sum_{i=1}^{n} w_i U(\xi, \xi_{r_i}). \tag{2}$$

The first part of the above equation, $b_0 + b_1 x + b_2 y + b_3 z$, forms a linear surface corresponding to an uniform or affine transformation, and the second part is nonlinear (non-uniform transformation). The input to the function is the coordinate location of a generic point $\xi = [x\ y\ z]^T$ in the reference workspace and $g(x,y,z)$ outputs the corresponding location $\xi_t = [x\ y\ z]^T$ in the deformed workspace. The coefficient vectors b_0 to $b_3 \in \mathbb{R}^{3\times 1}$ are constants to be determined later, w_i is a weighing coefficient for each of the n reference landmarks, and $U(\xi, \xi_{r_i})$ is a radial basis function defined as

$$U(r_{ij}) = r_{ij}^2 \ln(r_{ij}^2). \tag{3}$$

Here, the value $r_{ij} = \|\xi_i - \xi_j\|$ is the Euclidean distance between points ξ_i and ξ_j, and ln( ) denotes the natural logarithm function.

In order to quantify the relative amount of distortion required to match pairs of landmarks in the same workspace, let $K \in \mathbb{R}^{n\times n}$ be a symmetric matrix that summarizes the distances between the n reference landmarks ξ_r, defined as

$$K = \begin{bmatrix} 0 & U(r_{12}) & \dots & U(r_{1n}) \\ U(r_{21}) & 0 & \dots & U(r_{2n}) \\ \vdots & & \ddots & \vdots \\ U(r_{n1}) & U(r_{n2}) & \dots & 0 \end{bmatrix}, \tag{4}$$

where, for example, $U(r_{12})$ is the distance between ξ_{r_1} and ξ_{r_2} as given by (3). The spacing of landmarks is an important constraint because it requires more shape deformation between closely spaced landmarks than between landmarks located at a distance from one another.

Let $R \in \mathbb{R}^{n\times 4}$ be a matrix gathering the n landmark points of the reference workspace, i.e.,

$$R = \begin{bmatrix} 1 & 1 & \dots & 1 \\ \xi_{r_1} & \xi_{r_2} & \dots & \xi_{r_n} \end{bmatrix}^T. \tag{5}$$

To compute the weighing coefficient of each landmark point and the coefficient vectors b, let us define a new matrix $L \in$

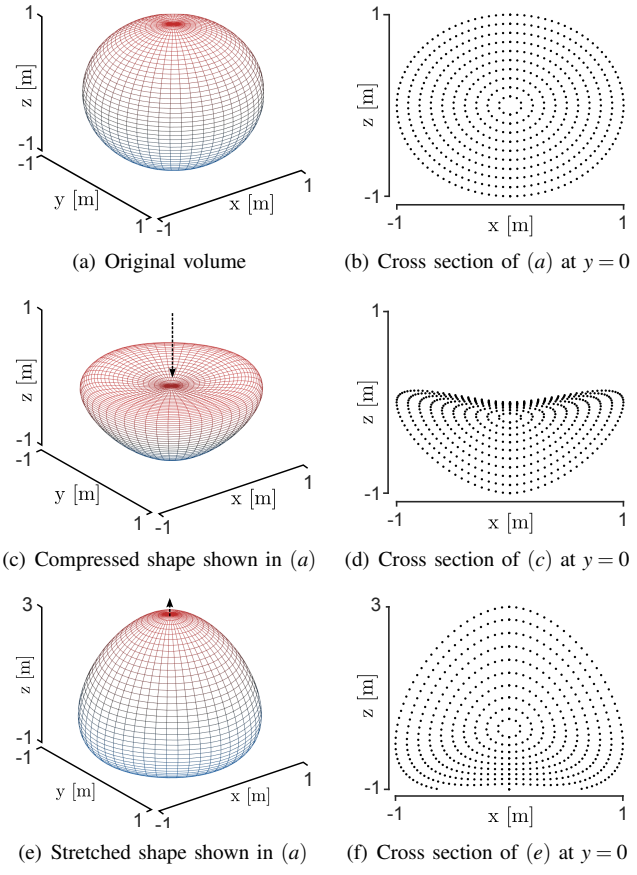

(a) Original volume (b) Cross section of (a) at $y = 0$

(c) Compressed shape shown in (a) (d) Cross section of (c) at $y = 0$

(e) Stretched shape shown in (a) (f) Cross section of (e) at $y = 0$

Fig. 2. Example of thin plate spline interpolation applied to a generic sphere. In (a) a sphere with unitary radius is created. In (b), a cross section of the sphere shows the internal points that compose the sphere at $y = 0$. The top landmark is moved from $[0,0,1]$ to $[0,0,0]$. In (c), the top landmark is moved from $[0,0,1]$ to $[0,0,3]$. Note that the scale in (e-f) is different, which adds to the distortion seen in the bottom of both images.

$\mathbb{R}^{(n+4)\times(n+4)}$ as

$$L = \begin{bmatrix} K & R \\ R^T & O_1 \end{bmatrix}, \tag{6}$$

where $O_1 \in \mathbb{R}^{4\times4}$ is a matrix of zeros. The inverse of L represents the energy required to displace the landmarks of the reference configuration in any combination and by any amount.

Since the reference landmarks must be displaced to match the target landmarks, let Q be a matrix containing the desired respective coordinates ξ_{t_i}, in the target configuration, of each reference landmark ξ_{r_i}, that is

$$Q = \begin{bmatrix} \xi_{t_1} & \xi_{t_2} & \dots & \xi_{t_n} & O_2 \end{bmatrix}^T,$$

where $O_2 \in \mathbb{R}^{4\times3}$ is a matrix of zeros concatenated here to give Q the same number of rows as L^{-1}.

Now, the n weights w_i assigned to the non-uniform modes of shape variation, and the vectors b_0 to b_2 that give the uniform part of the transformation are simply determined as follows:

$$[w_1 \ \dots \ w_n, \ b_0 \ b_1 \ b_2 \ b_3]^T = L^{-1}Q. \tag{7}$$

The new location of a generic point $\xi = [x \ y \ z]^T$ originally

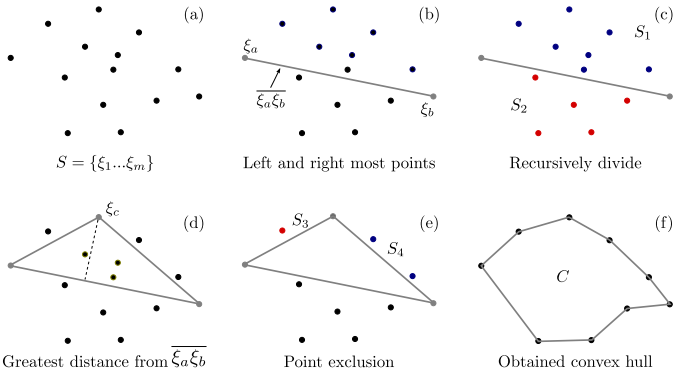

Fig. 3. Overview of the two-dimentional convex hull algorithm.

expressed in the reference workspace can now be calculated in the target workspace by inputting the result of (7) in (2). Notice that if the target landmarks location is a linear scaling of the reference landmarks location, i.e., $\xi_{t_i} = \lambda\xi_{r_i} \ \forall i$ with $\lambda \in \mathbb{R}$, then $w_i = 0 \ \forall i$ and the transformation is affine.

An example of the transformation applied to a sphere of unitary radius is presented in Fig. 2(a). Six landmarks are assigned on the surface of the sphere at $[0,0,1],[0;0,\text{-}1],[0,1,0],[0,\text{-}1,0],[1,0,0],[\text{-}1,0,0]$. The landmark on the lop of the sphere is then moved to the center ($[0,0,1] \rightarrow [0,0,0]$) while other landmarks are kept at their original locations. The resulting shape and the interpolated inner points are shown in 2(c) and 2(d). In 2(e) the top landmark is moved to $[0,0,3]$ and the inner points deform accordingly.

III. Workspace Identification

The next step toward mapping two workspaces is to define their limits, i.e., the set of reachable points in both ends of the teleoperation scheme. This set of points can be demonstrated by simply moving the end-effector of one robotic device arbitrarily while the three-dimensional position of the end-effector (coordinates on xyz, or rather $\xi = [x \ y \ z]^T$) is recorded. From this set of points, the limits of the workspace will be extracted. Next, points on the contours of each workspace will define the registration landmarks.

A. Convex Hull of Workspace Contours

Provided the cloud of reachable 3D points, a computational geometry algorithm known as Convex Hull is used to obtain the outlines of the workspace [16]. Given a of set points in the Euclidean space, the objective is to compute the smallest convex set containing all points in the set. The 3D position of the robot end-effector $\xi \in \mathbb{R}^3$ in the Cartesian coordinates is sampled with a fixed sampling time. Since the position samples are not evenly distributed along the workspace, as the velocity $\dot{\xi}$ is not constant, the dataset is down-sampled to m samples and forms the following dataset:

$$S_e = \{\xi_j \in \mathbb{R}^n\}_{j=1}^m \in \mathbb{R}^{m\times3}. \tag{8}$$

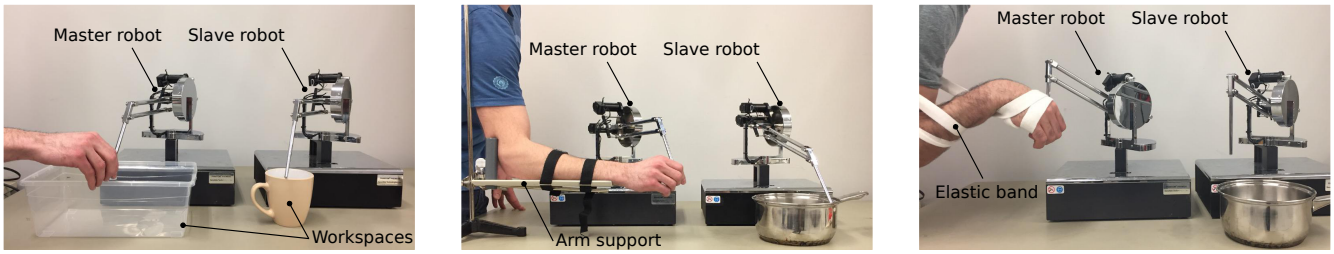

(a) Sceraio 1 - Object-to-object mapping (b) Scenario 2 - Wrist motion to object mapping (c) Scenario 3 - Shoulder motion to object mapping

Fig. 4. Experimental scenarios using an unilateral teleoperation scheme. Scenario 1 (*a*) maps the workspace of two objects. Scenarios 2 (*b*) and 3 (*c*) map the workspace achieved when the user can only move his wrist or shoulder joints, respectively, to that of the cylinder delineated by the pot.

Here the syntax j is the j^{th} sample of the demonstrated workspace containing m samples in total.

The convex hull of the set of points comprised in S in the three-dimensional space is the intersection of all convex sets containing all the points in S_e. In details for m points the convex hull of S, denoted C is given by

$$C \equiv \left\{ \sum_{j=1}^{m} \lambda_j \xi_j : \lambda_j \geq 0 \ \forall j \text{ and } \sum_{j=1}^{m} \lambda_j = 1 \right\}. \tag{9}$$

When $S = S_e$, the convex hull C defines the boundaries of the demonstrated workspaces.

A simplified two-dimensional version of the algorithm is systematised in Fig. 3. We begin by providing the set S of arbitrary scattered data points ξ (see (a)). The first operation consists in calculating the leftmost and rightmost points in the data set (ξ_a and ξ_b). These are guaranteed to be part of the solution (see (b)). Next, the line $\overline{\xi_a \xi_b}$ is formed to connect these points and divide the data set into two different parts. Points lying in the left of this line are considered one subset (S_2) and the remaining points are considered as another subset (S_1 in (c)). Both S_1 and S_2 are processed recursively. In this example, only S_1 will be further treated but the S_2 would be handled in the same way.

The algorithm continues by identifying the point with the greatest distance from the line $\overline{\xi_a \xi_b}$, called ξ_c in (d). This point connects to the limits of the line to form a triangle. Points lying within the triangle are discarded as they evidently are not part of the convex hull (see (e)). The recursive process in then repeated. Points in the right and left of the triangle form new subsets S_3 and S_4. The process continues until the segment $\overline{\xi_a \xi_b}$ is no longer part of the hull polygon as shown in (f).

For simplicity, the 3D problem will be approximated by a series of 2D convex hulls, each of which deals with points having the same coordinates along z in S_e or width (position along x) in S_e. Each convex hull then represents the contour of a horizontal or vertical cross section of the volume formed by the points in S_e. Combined, the set of 2D convex hulls outlines the 3D contours of the workspaces described in S_e.

B. Defining Registration Landmarks

The next step required in the mapping process is to define pairs of landmarks pertaining to the contours of each workspaces that are to be matched through the transformation described in Section II. To this end, we start by normalizing the 3D convex hulls obtained on the master and slave robot, i.e., dividing the coordinates x, y, and z of each vertex in the convex hull by the maximum width, depth, and height of the hull, respectively. Next, we center the median of each convex hull such that they center at the origin O of a hypothetical xyz frame.

The principle here is that a vector that connects a landmark point in one workspace to the center of its hull, must have a similar orientation as in the other workspace. With this in mind, an intuitive and simple approach to define the landmarks is to construct a series of straight lines L_j with $j = \{1, 2, ..., d\}$, each of which starts at the median of each centred convex hull (O) and ends at a point ξ_ℓ defined in spherical coordinates as

$$\xi_\ell = \begin{bmatrix} x_\ell \\ y_\ell \\ z_\ell \end{bmatrix} = \begin{bmatrix} \sin(\vartheta)\cos(\varphi) \\ \sin(\vartheta)\sin(\varphi) \\ \cos(\vartheta) \end{bmatrix} \rho, \tag{10}$$

where $\rho = \sqrt{3}$ is the line length $\forall j$, ϑ is the polar angle formed with the z axis, φ is the azimuthal angle with respect to x. If the lines are equally distributed in space, the spherical coordinates are within the following range

$$\vartheta, \varphi = \frac{2\pi}{d} k + c, \text{with } k \in \{1, 2, ..., d\}, \ d \in \mathbb{N}^*. \tag{11}$$

Thus, considering all possible combinations of ϑ and φ, the total number of lines is d^2 provided that the constant c is different in ϑ and φ.

These lines are drawn within each convex hull and each of them will intersect the convex hull surface at a certain point. See Fig. 5(c) for an example. As a consequence, the pair j of landmarks, pertaining each to one workspace contour, is simply given by the points where the line L_j intersects C in each workspace. At the end of the process, the total number of reference landmarks pairs is d^2.

IV. Experimental Validation

An unilateral teleoperated scheme using two haptic devices (Phantom Premium 1.5A from Geomagic, Durham, USA) is used to validate the proposed approach (see Fig. 4). Demonstration of each workspace is performed by moving the end-effector of each robot within the desired range of motion.

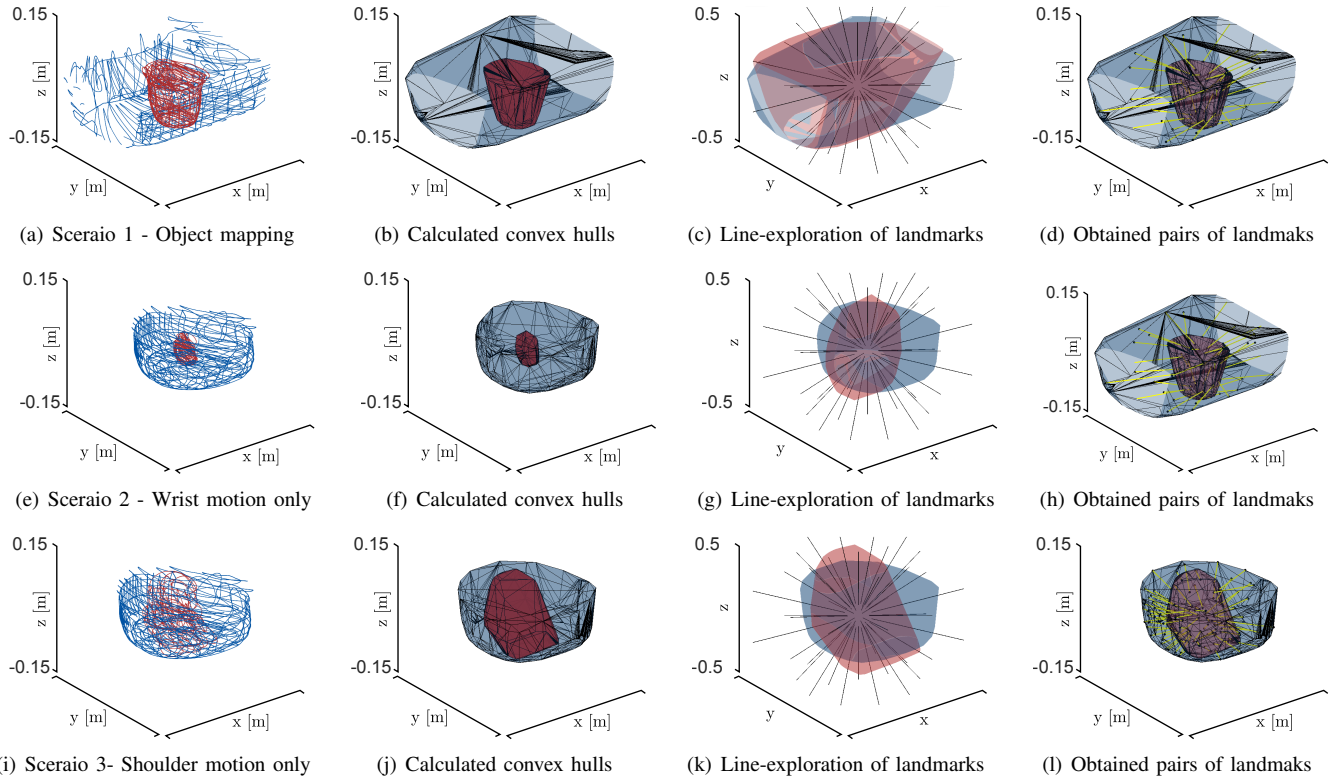

(a) Sceraio 1 - Object mapping (b) Calculated convex hulls (c) Line-exploration of landmarks (d) Obtained pairs of landmaks

(e) Sceraio 2 - Wrist motion only (f) Calculated convex hulls (g) Line-exploration of landmarks (h) Obtained pairs of landmaks

(i) Sceraio 3- Shoulder motion only (j) Calculated convex hulls (k) Line-exploration of landmarks (l) Obtained pairs of landmaks

Fig. 5. Demonstration, outline of the workspaces, and assignment of landmark points in each scenario. The first column shows the raw demonstrated data S_e. The second column shows the calculated convex hulls. In the third column the normalized workspaces and the landmark lines are drawn. The yellow lines in the last column indicate the obtained pair of landmarks once the convex hulls are scaled back to their original size.

Once the workspace mapping is obtained, the transformed position of the master robot end-effector serves as the desired position of the slave robot, which is controlled through a proportional-integral-derivative controller. Note that in unilateral tele-operation, force-feedback is not implemented.

Three experimental scenarios are considered.

Scenario 1: See Fig. 4(a). In this scenario, we are interested in downscaling the workspace delineated by a rectangular plastic container to that of a mug. The idea is to refine the user's motion allowing for precise execution of movements within the smaller workspace. This scenario can be considered for patients with movement spasms. To obtain the workspaces, the end-effector of the master and slave robot are manually moved around within the limits of the container and the mug, respectively, for approximately 45 seconds.

Scenario 2: See Fig. 4(b). In this scenario we map the workspace obtained when the user is only able to move his wrist (in all directions, creating a volume) to that of a round object, such as a pot. The arm of an individual without disability is fixed to the support shown in the figure and the individual moves his wrist such that the workspace of the master robot can be acquired in the same way as in Scenario 1 except that the workspace boundaries are determined by the wrist physical limits.

Scenario 3: See Fig. 4(c). Here, the forearm and the wrist of a individual without disability are tied to his humerus using an elastic band such that the individual is only able to move the end-effector of the robot through movements of his shoulder joints. The obtained workspace is then up-scaled to that of the same object as in Scenario 2.

The demonstrated workspaces and the sequence used to obtain the pairs of landmarks is shown in Fig. 5. The first column is the set of demonstrated points S_e of each workspace overlaid in the same graph, for each scenario. The second column shows the convex hulls calculated for each set of points. The normalized workspace and the landmark searching lines can be seen in the third column. The last column shows the obtained pairs of landmarks that are be used to deform the workspace of the master robot to that of the slave robot following the direction of the yellow lines using $d = 10$ in Equation (11).

Experimental results are summarized in Fig. 6. In (a) (left) the user delineates the contours of the plastic container by moving the master robot end-effector. The slave robot trajectory is shown in the right-hand-side panel. Four trials presented for each scenario (shown by different colors) demonstrate that the proposed mapping spans workspaces with different geometries with reasonable accuracy. In (b) the user can only move his wrist, as in Scenario 2, and attempts to outline the contours of the pot at different heights using the master robot. As the height changes, it can be seen that the required wrist movement reduces according to the workspace limits. The experimental results shown (c) are similar to those in (b), except that the user is only able to move the shoulder, as in

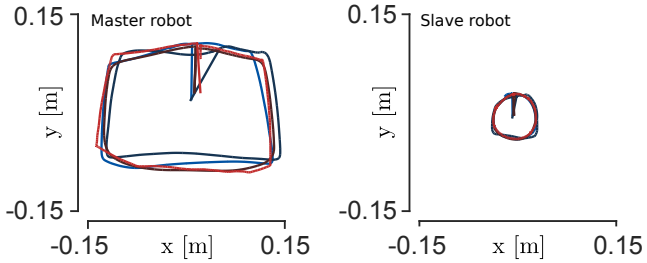

(a) Scenario 1 - Object contour mapping

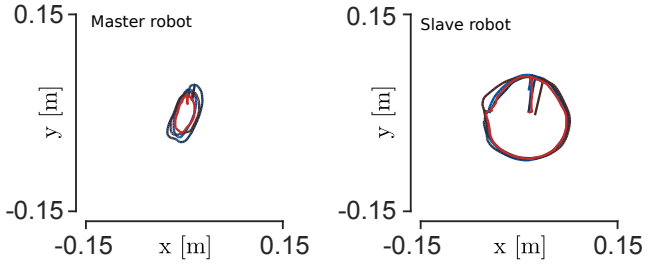

(b) Scenario 2 - Outlining object contours at different heights

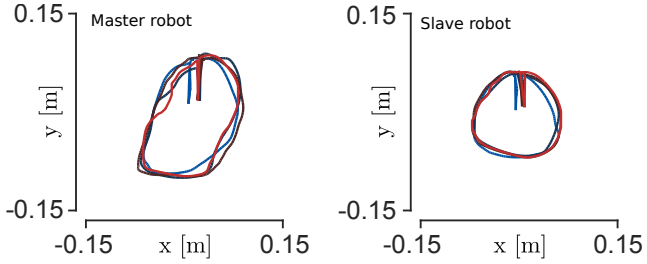

(c) Scenario 3 - Outlining the object contours

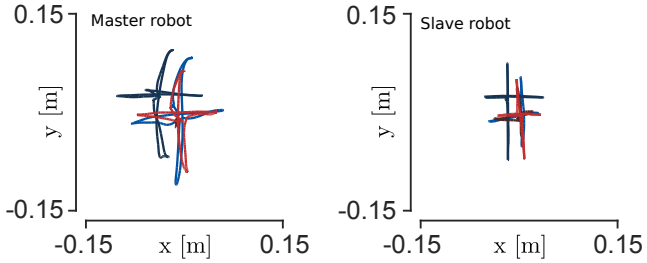

(d) Scenario 3 - Drawing straight lines

Fig. 6. Experimental results using unilateral teleoperation in each scenario.

Scenario 3. In (d), Scenario 3 is again considered. Rather than outlining contours, the user draws straight lines in the slave robot 'sworkspace. It can be seen that the mapping is nonlinear close to the boundaries of the workspace but maintains good linearity in the center of the workspace.

V. Conclusion and Perspectives

This paper proposes a nonlinear workspace mapping between the patient's range of motion and that of the object to be explored through teleoperation. It may be used to refine the patient's motion and reduce effects of tremor and spasms, but also to upscale the range of motion to match the size of the object. One may envision a scenario where the patient interacts with different objects, each of which has its own workspace spanning the patient's range of motion. In that way, the patient is always using his entire workspaces, which is expected to promote patient engagement.

There are several ways to improve upon the presented methodology. In order to match the patient's preferred direction of motion, an additional step may be used in the scaling process to rotate the workspaces and adjust the direction of motion from one workspace to another. In this regards, the assignment of landmarks also plays an important role. An alternative to the searching-lines approach presented here may be to consider the Euler angles of all vertex points in each convex hull, and then iteratively form pairs of points considering those with similar angles such that the distortion of the workspace given by Equation (1) is minimized, or until a defining workspace feature such as a straight line can be scaled without distortion. In addition, one may consider filtering the demonstrated points in an attempt to minimize the effects of potential outliers that can negatively affect the mapping accuracy. Future work will also study the effects of nonlinear mapping on the stability of bilateral teleoperation.

References

[1] H. Krueger et al., "Prevalence of individuals experiencing the effects of stroke in canada," *Stroke*, vol. 46, no. 8, pp. 2226–2231, 2015.

[2] A. Rios et al., "Playfulness in children with limited motor abilities when using a robot," *Physical & Occupational Therapy in Pediatrics*, vol. 36, no. 3, pp. 232–246, 2016.

[3] N. Paneth, T. Hong, and S. Korzeniewski, "The descriptive epidemiology of cerebral palsy," *Clinics in Perinatology*, vol. 33, no. 2, pp. 251–267, 2006.

[4] H. van der Ploeg et al., "Physical activity for people with a disability," *Sports Medicine*, vol. 34, no. 10, pp. 639–649, 2004.

[5] V. Maheu et al., "Evaluation of the jaco robotic arm: Clinico-economic study for powered wheelchair users with upper-extremity disabilities," in *International Conference on Rehabilitation Robotics*, 2011, pp. 1–5.

[6] R. Alqasemi and R. Dubey, "Maximizing manipulation capabilities for people with disabilities using a 9-DOF wheelchair-mounted robotic arm system," in *International Conference on Rehabilitation Robotics*, 2007, pp. 212–221.

[7] F. Conti and O. Khatib, "Spanning large workspaces using small haptic devices," in *Eurohaptics Conference*, 2005, pp. 183–188.

[8] N. Pernalete et al., "Development of a robotic haptic interface to assist the performance of vocational tasks by people with disabilities," in *International Conference on Robotics and Automation*, vol. 2, 2002, pp. 1269–1274.

[9] K. Adams, L. Alvarez, and A. Rios, "Robotic systems for augmentative manipulation to promote cognitive development, play, and education," in *Robotic Assistive Technologies: Principles and Practice*. CRC Press, 2017, pp. 219–260.

[10] J. Vauclair, "Phylogenetic approach to object manipulation in human and ape infants," *Human Development*, vol. 27, no. 5-6, pp. 321–328, 1984.

[11] N. Maclean and P. Pound, "A critical review of the concept of patient motivation in the literature on physical rehabilitation," *Soc Sci Med*, vol. 50, no. 4, pp. 495–506, 2000.

[12] M. Najafi et al, "Robotic assistance for children with cerebral palsy based on learning from tele-cooperative demonstration," *International Journal of Intelligent Robotics and Applications*, pp. 1–12, 2017.

[13] A. Cook, P. Encarnação, and K. Adams, "Robots: Assistive technologies for play, learning and cognitive development," *Technology and Disability*, vol. 22, no. 3, pp. 127–145, 2010.

[14] J. Noth, "Trends in the pathophysiology and pharmacotherapy of spasticity," *Journal of neurology*, vol. 238, no. 3, pp. 131–139, 1991.

[15] F. Bookstein, "Principal warps: Thin-plate splines and the decomposition of deformations," *Transactions on Pattern Analysis and Machine Intelligence*, vol. 11, no. 6, pp. 567–585, 1989.

[16] B. Barber, D. Dobkin, and H. Huhdanpaa, "The quickhull algorithm for convex hulls," *Transactions on Mathematical Software*, vol. 22, no. 4, pp. 469–483, 1996.